Paper No.
11195

NACE INTERNATIONAL CORROSION 2018 Conference & Expo

Criteria for Protective Film Growth on Carbon Steel Rebar in a Carbonation Process

Yoon-Seok Choi, K. Channa R. De Silva, Xiang Yong, David Young, Srdjan Nesic
Institute for Corrosion and Multiphase Technology,
Department of Chemical and Biomolecular Engineering, Ohio University
342 West State Street
Athens, OH 45701
USA

ABSTRACT

The motivation behind this research was to determine if an iron carbonate ($FeCO_3$) layer can be effective for prevention of CO_2 corrosion of steel rebars, associated with production and use of carbonated calcium silicate cement-based concrete. Laboratory scale experiments were conducted on optimizing the conditions utilized to form a protective $FeCO_3$ layer on reinforcement steel by controlling solution chemistry, temperature, and surface condition. Subsequently, the rebar with protective layers formed under different conditions was exposed to a 3.5 wt.% NaCl solution in air, representative of an extreme service condition. The corrosion rates were assessed electrochemically using the linear polarization technique. The surface morphologies of the steel and coating were analyzed by scanning electron microscopy (SEM), energy dispersive X-ray spectroscopy (EDS), and Raman spectroscopy. Iron carbonate formed on sandblasted rebar had the lowest corrosion rates (<0.2 mm/y) under the service condition, while the other surface conditions comprising of a mill scale had corrosion rates in excess of 0.3 mm/y. Future work will emphasize modifying the iron carbonate coating to counter its susceptibility to degradation in oxidizing environments.

Key words: Concrete, carbonation, steel rebar, CO_2 corrosion, $FeCO_3$ coating

INTRODUCTION

Emissions from cement production associated with concrete represent a significant source of carbon dioxide (CO_2) emissions.[1] Thus, there has been increasing awareness of the need to reduce emissions of CO_2 during cement manufacturing. Taking into account that 60% of the CO_2 emissions in cement production come from the use of limestone, lowering the usage of this material is a promising way to reduce the carbon footprint of the process.[2] Success was achieved related to production of cement that involves curing into concrete in a CO_2/water environment by a carbonation process.[3,4] This can dramatically reduce CO_2 emissions associated with concrete production, as well as provide a useful bulk application for captured CO_2.

Steel rebar embedded in Ordinary Portland Cement (OPC) concrete is usually protected from corrosion by a thin oxide layer that is formed, and maintained, on their surfaces because of the highly alkaline environment of the surrounding concrete (pH 13).[5,6] However, the concrete produced by the carbonation process could lead to steel rebar corrosion because of a lower pore water pH (~ 9) compared to OPC concretes, making it difficult to maintain a stable passive layer.[2,4] On the other hand, there is a possibility to form a protective corrosion product layer on steel rebar during the curing process since the environment has CO_2 and water, which favors the formation of iron carbonate ($FeCO_3$).

This layer of $FeCO_3$, also known as siderite, forms on the steel surface and confers some protection by slowing down the corrosion process as a result of mass transfer resistance set by the layer, blocking the steel surface and making it unavailable for corrosion. Solid $FeCO_3$ forms when the concentrations of Fe^{2+} and CO_3^{2-} exceed the solubility limit according to the following reaction:[7-9]

$$Fe^{2+}_{(aq)} + CO_3^{2-}{}_{(aq)} \leftrightarrow FeCO_{3(s)} \quad (1)$$

The precipitation rate of $FeCO_3$ depends on its saturation level, which is defined by:

$$S_{FeCO_3} = \frac{c_{Fe^{2+}} \cdot c_{CO_3^{2-}}}{K_{sp}} \quad (2)$$

where, $c_{Fe^{2+}}$ is the ferrous ion concentration, $c_{CO_3^{2-}}$ is the carbonate ion concentration, and K_{sp} is the solubility limit of $FeCO_3$. $FeCO_3$ will not form if the saturation level is less than 1. The degree of protection that the $FeCO_3$ layer provides has been investigated as a function of shear stress, adhesion properties, dissolution in flowing conditions, and other parameters.[10-13] However, limited research has been done on the stability of $FeCO_3$ with respect to the environments associated with production and use of carbonated calcium silicate cement-based concrete.

Thus, the objective of this study was to optimize the condition for $FeCO_3$ formation on steel rebar during the curing process and to evaluate the stability of $FeCO_3$ under service conditions.

EXPERIMENTAL PROCEDURE

In order to simulate conditions suitable for the formation of a protective $FeCO_3$ on a steel rebar surface in an aqueous environment, several parameters were adjusted including pH, temperature, solution chemistry, initial Fe^{2+} concentration, and steel rebar specimen surface condition. Table 1 shows the test matrix for $FeCO_3$ forming conditions. After forming $FeCO_3$ on the steel rebar specimen surface, the specimen was moved to a glass cell with 3.5 wt.% NaCl which simulates the service conditions, in order to evaluate the stability of $FeCO_3$. Table 2 shows the test matrix for the service conditions.

Experiments for both $FeCO_3$ forming and service conditions were conducted in a 2 L glass cell with a three electrode electrochemical setup (Figure 1). A Pt mesh electrode was used as the counter electrode and a saturated Ag/AgCl electrode was employed as the reference electrode. Cooling water was circulated in the condenser to minimize the evaporation of the aqueous solution in the glass cell at high temperature. The pH value was monitored by a pH meter. The solution pH was adjusted by $NaHCO_3$ and NaOH; deionized (DI) water being used for electrolyte preparation. The solution was purged with the CO_2 or open to air, depending on the test conditions. Open-circuit potential (OCP) and linear polarization resistance (LPR) measurements were used to monitor the corrosion behavior of steel rebar specimen with time. After the completion of each test, cross-sections and surfaces of the steel rebar specimen were analyzed using SEM, EDS, and Raman spectroscopy.

Table 1
Test matrix for $FeCO_3$ forming conditions.

	Material	pH	Temperature (°C)	Solution	Initial Fe^{2+} concentration (ppm)	CO_2 partial pressure (bar)	Exposure period (day)
1	As-received rebar	9	90	DI water	0	0.4	3
2	As-received rebar	6.6	80	DI water	50	0.5	2
3	Sandblasted rebar	6.6	80	DI water	50	0.5	2

Table 2
Test matrix for simulating service condition.

	Material	pH	Temperature (°C)	Solution	CO_2 partial pressure (bar)	Exposure period (day)
A	$FeCO_3$ formed by condition 1	8.5	25	3.5 wt.% NaCl	0 (open to air)	5
B	$FeCO_3$ formed by condition 2					
C	As-received rebar					
D	$FeCO_3$ formed by condition 3					
E	Sandblasted rebar					

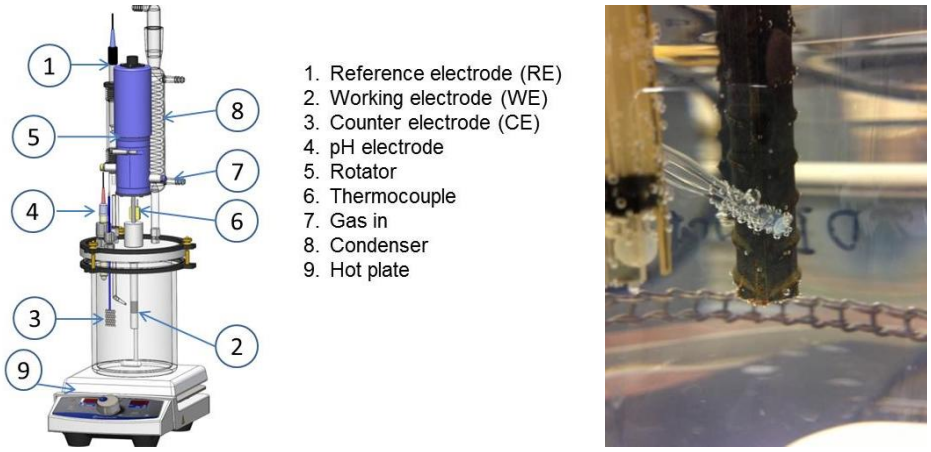

(a) (b)

Figure 1: Experimental setup for $FeCO_3$ formation and stability test: (a) schematic of glass cell system, (b) picture of steel rebar in the glass cell.

RESULTS AND DISCUSSION

Condition 1 (as-received rebar, pH 9, 90°C)

Figure 2 shows the variations of corrosion rate and OCP with time for rebar exposed to the $FeCO_3$ formation conditions (pH 9, 90°C). There was a sharp decrease in the corrosion rate over the initial 10 hours, then the corrosion rate remained stable at a value of around 0.05 mm/y. The OCP of the rebar sharply increased from -0.4 V to -0.2 V in the first 12 hours and stabilized at -0.3 V.

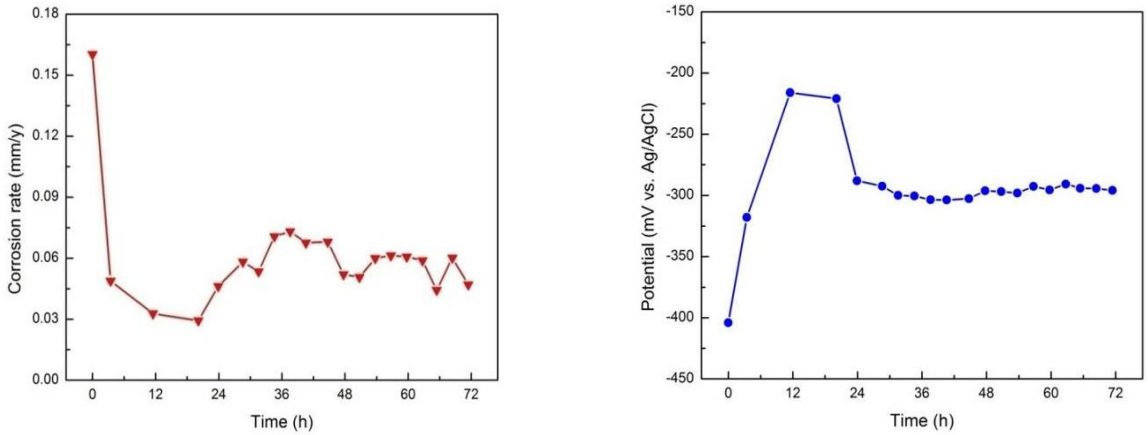

(a) (b)

Figure 2: Variations of (a) corrosion rate and (b) corrosion potential with time for the as-received steel rebar under $FeCO_3$ formation conditions 1 (pH 9, 90ºC).

Figure 3 shows the SEM image and EDS spectra of the specimen surface after 72 hours of exposure in the pH 9 solution at 90ºC. It can be seen that the surface was covered by corrosion product, consisting of Fe, C and O. Figure 4 shows a Raman spectrum of the corrosion product layers. The corrosion products were mainly composed of magnetite and hematite, identifying the layer as mill scale. There is no vibrational mode at *ca.* 1086 cm^{-1}, which means that $FeCO_3$ is absent from the corrosion products.

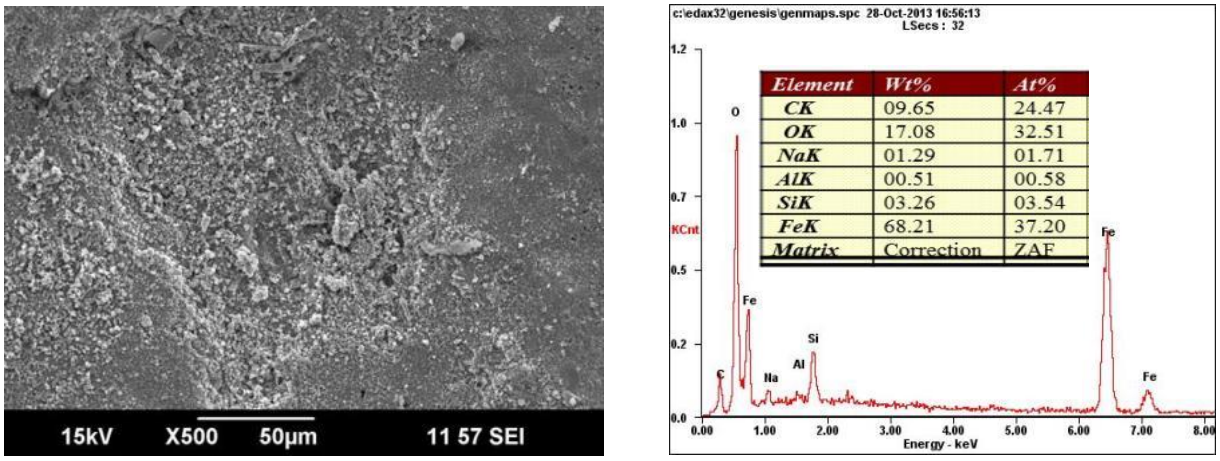

(a) (b)

Figure 3: SEM image (a) and EDS spectra (b) of the as-received rebar surface exposed to a pH 9 solution at 90ºC for 72 hours.

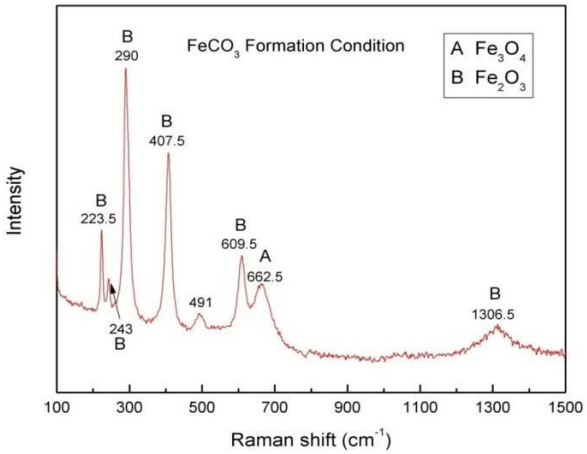

Figure 4: Result of Raman spectroscopy analysis for the specimen exposed to pH 9, 90ºC for 72 hours.

After 72 hours of immersion, the rebar specimen was withdrawn from the solution, washed, dried and then exposed to the service conditions (3.5% wt. NaCl solution, pH 8.5, 25ºC). Figure 5 shows the variations of corrosion rate and OCP with time for the rebar specimen exposed to the service conditions. The corrosion rate increased with time from 0.15 mm/y to 0.5 mm/y and the OCP value decreased to a lower value compared to the initial value. This indicates that the oxide layer formed at pH 9, 90ºC with mill scale is unprotective under the service conditions.

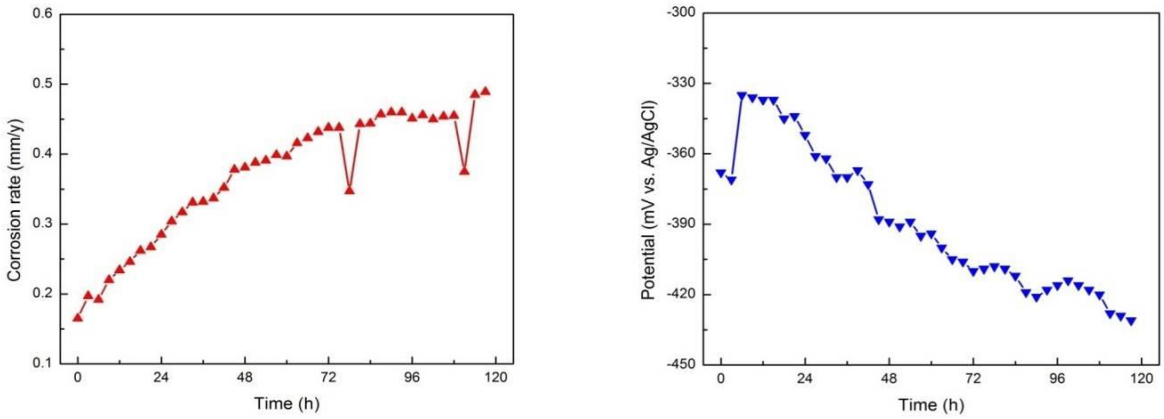

(a) (b)

Figure 5: Variations of (a) corrosion rate and (b) corrosion potential with time for the steel rebar under service conditions (3.5 wt.% NaCl, pH 8.5, 25ºC).

After exposing the steel rebar in the service conditions for 120 hours, the specimen surface was observed by SEM and EDS. It is interesting to note that crystalline corrosion products accumulated on the specimen surface, had a morphology similar to $FeCO_3$, as demonstrated in Figure 6.

The Raman spectroscopy result of the rebar surface after exposing to the service conditions is shown in Figure 7. There is a vibration mode at 1083 cm^{-1}, which indicates the existence of a carbonate product, most probably $FeCO_3$. The $FeCO_3$ was generated probably due to the presence of CO_3^{2-} ions from $NaHCO_3$ used to adjust the solution pH. However, it seems to be unprotective based on the corrosion rates shown in Figure 5.

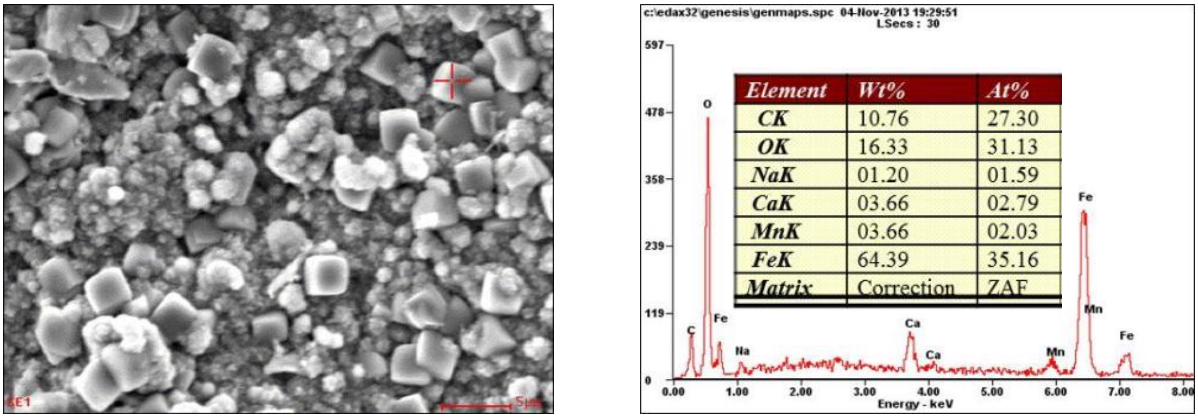

(a) (b)

Figure 6: SEM image (a) and EDS spectra (b) of the rebar surface exposed to the service conditions (3.5 wt.% NaCl, pH 8.5, 25°C) for 120 hours.

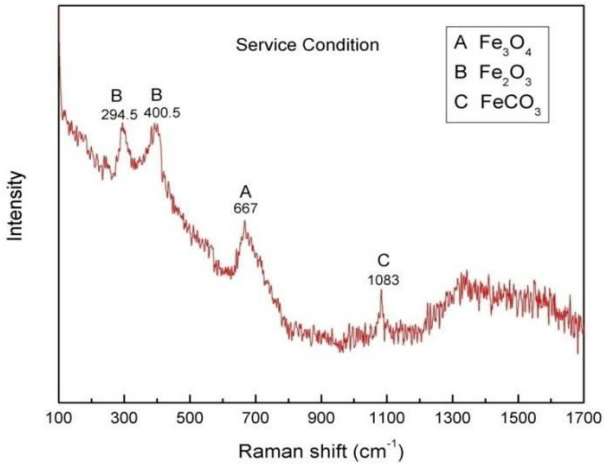

Figure 7: Result of Raman spectroscopy analysis for the specimen exposed to the service conditions for 120 hours.

Condition 2 (as-received rebar, pH 6.6, 80°C, 50 ppm Fe^{2+})

Based on the result from Condition 1, in order to obtain a $FeCO_3$ layer on the rebar specimen surface, it was necessary to reduce the pH and temperature. A typical condition for $FeCO_3$ layer formation in CO_2 corrosion research is 80°C, 50 ppm Fe^{2+}, 1 wt.% NaCl and pH 6.6.[14]

The corrosion rate and OCP variations of the as-received rebar in the newly selected $FeCO_3$ formation conditions is demonstrated in Figure 8. The corrosion rate decreased with time and then stabilized at a low value of around 0.04 mm/y, while the OCP increased with time.

Figure 9 shows the SEM image and EDS spectrum of the specimen surface after 36 hours of exposure in the 1 wt.% NaCl solution (pH 6.6, 80°C). It can be seen that the surface was covered by crystalline corrosion product (morphology typical of $FeCO_3$), consisting of Fe, C and O. The specimen surface was also analyzed by Raman spectroscopy, an acquired spectrum being shown in Figure 10. The strong peaks at 279.86 and 1083.78 cm^{-1} indicate the presence of $FeCO_3$. Figure 11 shows the SEM images and EDS spectra of the cross-section of the specimen after 36 hours of exposure in the 1 wt.% NaCl solution (pH 6.6, 80°C). It clearly demonstrates a thin outer layer and a thick inner layer. Based on the results of surface analysis, the outer layer can be identified as $FeCO_3$ and the inner layer is the mill scale. The thickness of the $FeCO_3$ layer is around 4 µm, while the thickness of the mill scale layer is around 33 µm.

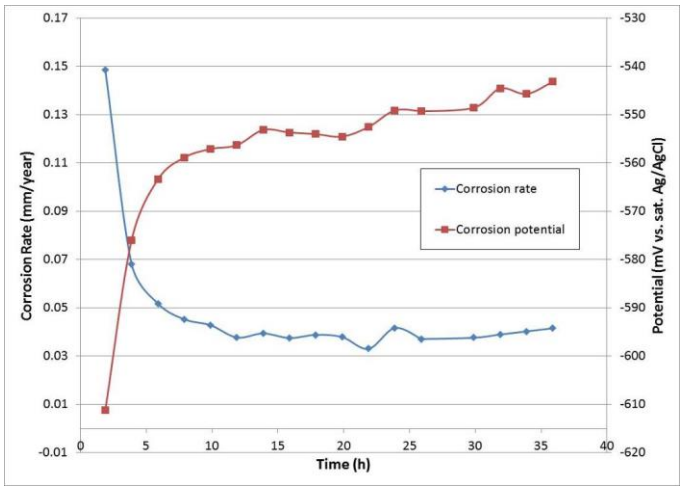

Figure 8: Variations of corrosion rate and corrosion potential with time for the as-received steel rebar under $FeCO_3$ formation conditions 2 (pH 6.6, 80ºC, 50 ppm Fe^{2+}).

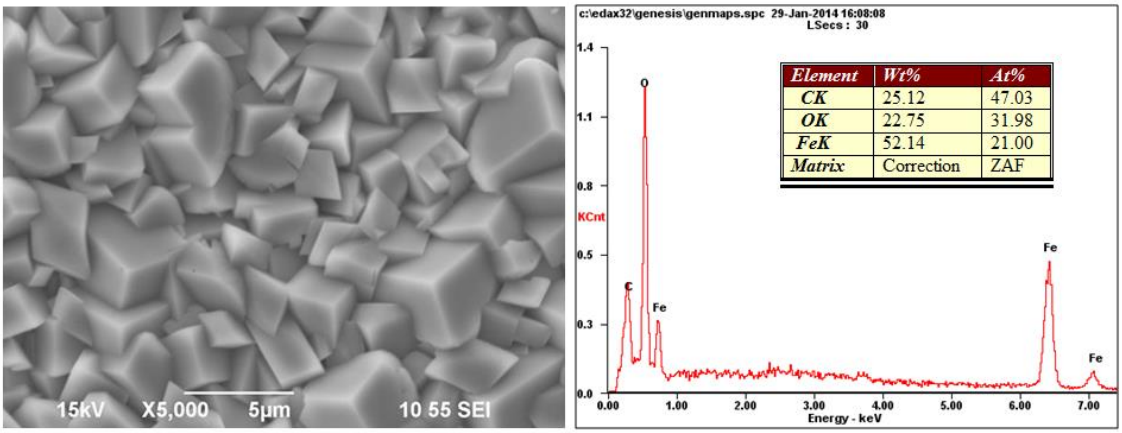

(a) (b)

Figure 9: SEM image (a) and EDS spectra (b) of the as-received rebar surface exposed to a pH 6.6 solution at 80ºC for 36 hours.

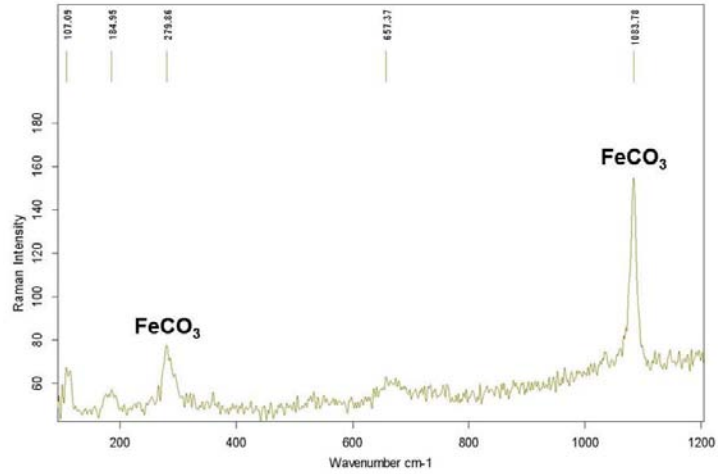

Figure 10: Result of Raman spectroscopy analysis for the specimen exposed to pH 6.6, 80ºC for 36 hours.

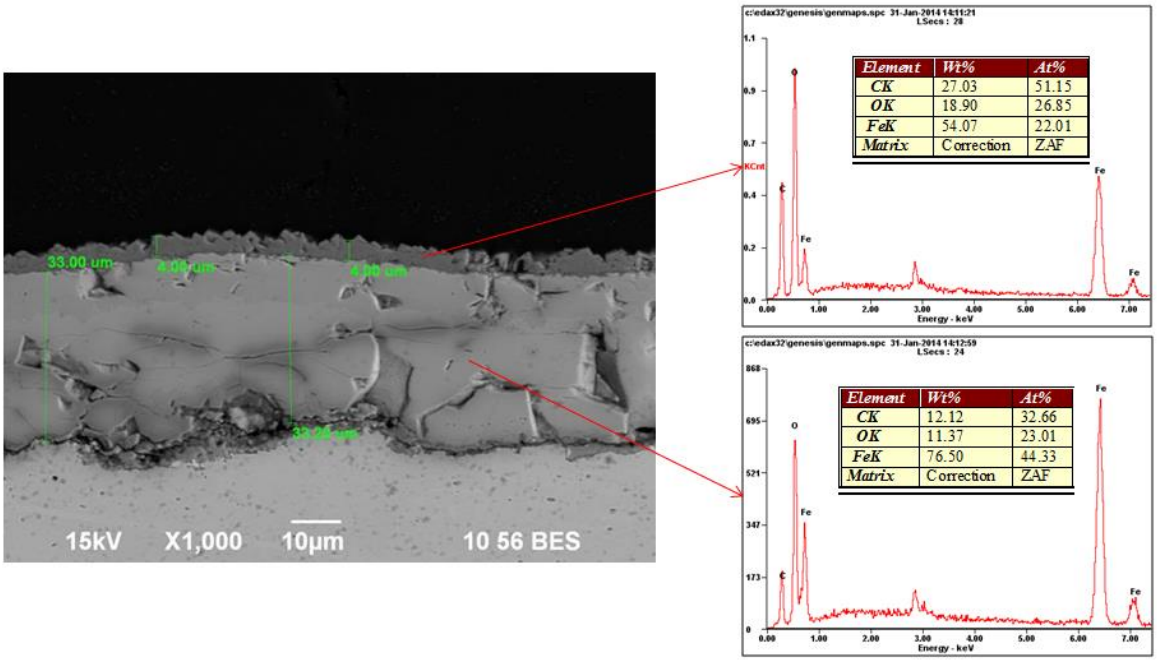

Figure 11: SEM image and EDS spectra of the cross-section of the as-received rebar exposed to a pH 6.6 solution at 80ºC for 36 hours.

When the rebar specimen with both $FeCO_3$ and mill scale was moved to the service condition, the corrosion rate increased with time and the corrosion potential decreased with time, as demonstrated in Figure 12. The final corrosion rate after 120 hours exposure was around 0.4 mm/y, which is a little less than the one shown in Figure 5 due to the $FeCO_3$ contributing some degree of protectiveness.

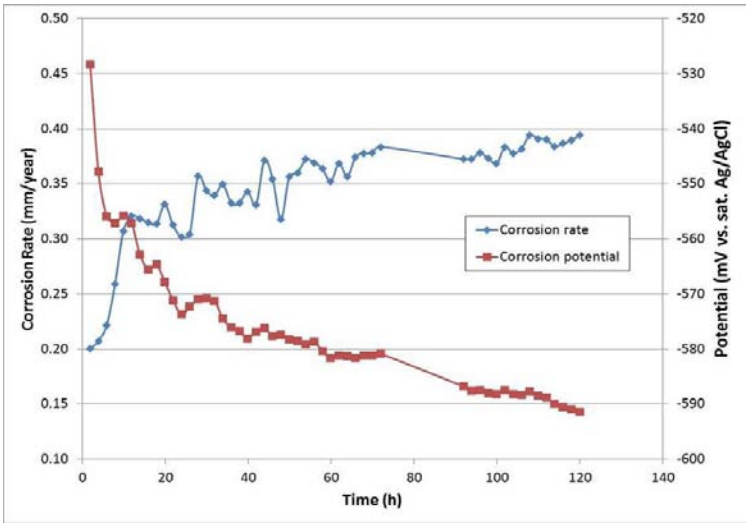

Figure 12: Variations of corrosion rate and corrosion potential with time for the steel rebar under service conditions (3.5 wt.% NaCl, pH 8.5, 25ºC).

Figure 13 shows the SEM image and EDS spectra of the surface of steel rebar after exposing to the service conditions for 120 hours. It can be seen that the outer $FeCO_3$ layers has been compromised during the exposure to the service conditions. The EDS result shows that the center section in the image had a lower concentration of C compared with the bottom right corner region, indicating a breakdown of the $FeCO_3$ layer.

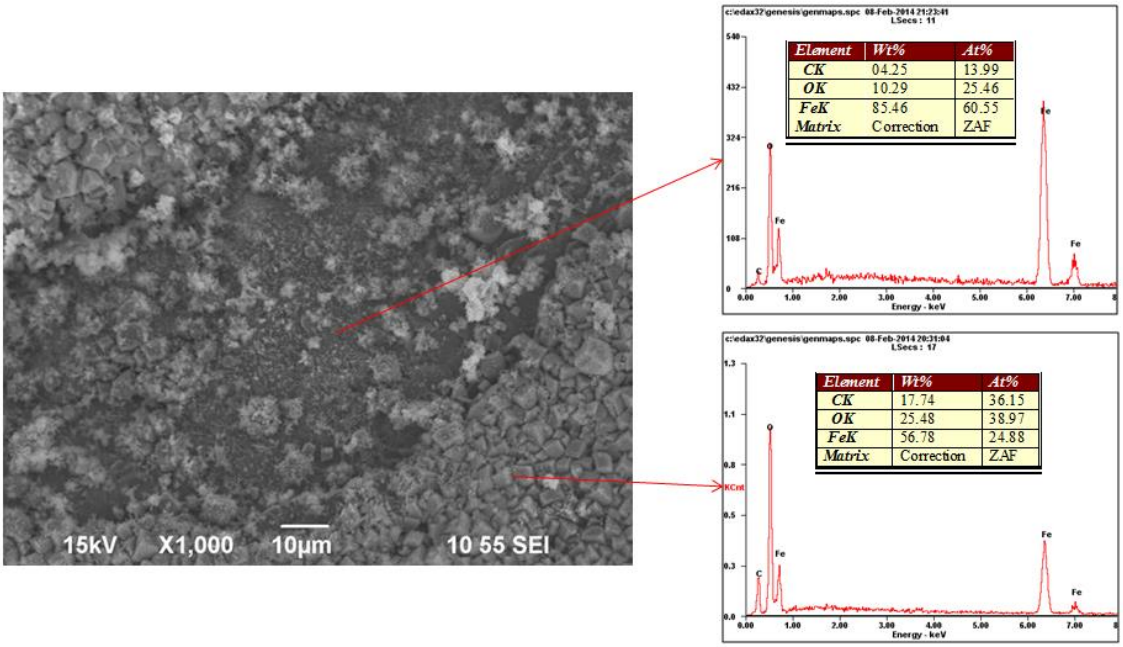

Figure 13: SEM image and EDS spectra of the surface of the rebar exposed to the service conditions for 120 hours.

In order to evaluate the effect of $FeCO_3$ formed on mill scale in the previous experiment, the as-received rebar was directly exposed to the service conditions. The variations of corrosion rate and OCP with time are shown in Figure 14. Both corrosion rate and corrosion potential decreased with time and then stabilized. Comparing with the specimen with both $FeCO_3$ and mill scale (Figure 12), the stabilized final corrosion rates did not show a significant difference, which means that the protectiveness of the $FeCO_3$ layer was only slight. The presence of the $FeCO_3$ layer showed some protectiveness in the initial stages of exposure, but this effect vanished due to the degradation of the $FeCO_3$ layer. As shown in Figure 15, the mill scale was removed locally after exposing to the service conditions for 120 hours. However, it is hard to reach a conclusion that this fault in the mill scale was present in the original as-received rebar specimen or if was a result of degradation occurred during the exposure to the service conditions.[15]

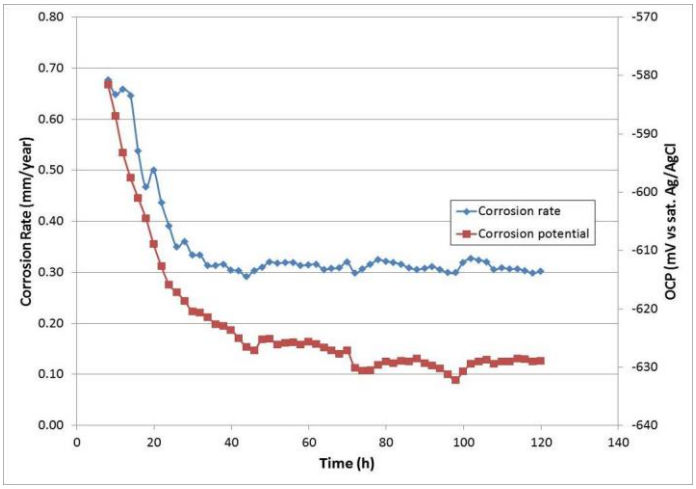

Figure 14: Variations of corrosion rate and corrosion potential with time for the as-received steel rebar under service conditions (3.5 wt.% NaCl, pH 8.5, 25ºC).

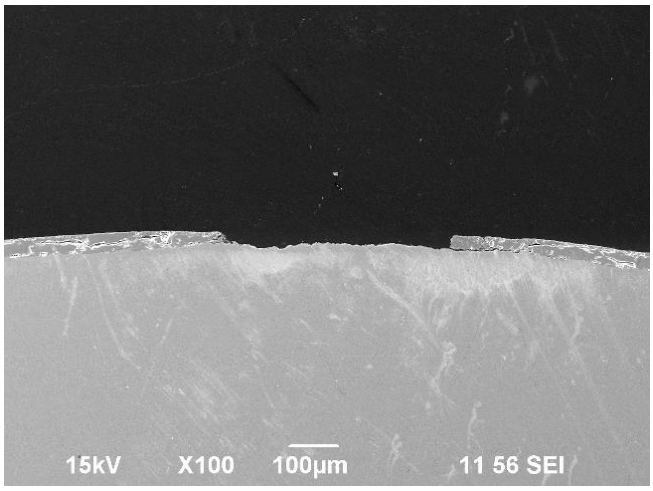

Figure 15: SEM image of the cross-section of the as-received rebar exposed to the service conditions for 120 hours.

Condition 3 (sandblasted rebar, pH 6.6, 80ºC, 50 ppm Fe^{2+})

In the current condition, the mill scale was mechanically removed by sandblasting before forming the $FeCO_3$ on the steel rebar surface. Figure 16 demonstrates the variations of corrosion rate and OCP of the sandblasted rebar in the $FeCO_3$ formation conditions (80°C, 50 ppm Fe^{2+}, 1 wt.% NaCl and pH 6.6). The corrosion rate decreased with time from an initial value of around 1 mm/y to a final stable value of around 0.03 mm/y. The corrosion potential sharply increased with time in the first 20 hours, and then decreased to a stable value. The increase of the OCP indicates that some protective layer formed on the specimen surface.

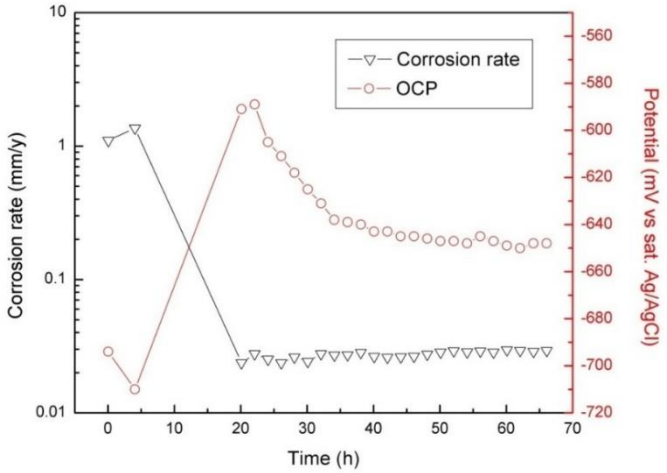

Figure 16: Variations of corrosion rate and corrosion potential with time for the sandblasted steel rebar under $FeCO_3$ formation conditions (pH 6.6, 80ºC, 50 ppm Fe^{2+}).

Figure 17 and Figure 18 show the results of SEM and EDS analyses for the sandblasted specimen surface and cross-section after exposing to the $FeCO_3$ formation condition. A compact and uniform $FeCO_3$ layer was found on the sandblasted rebar surface with a thickness of around 5 µm.

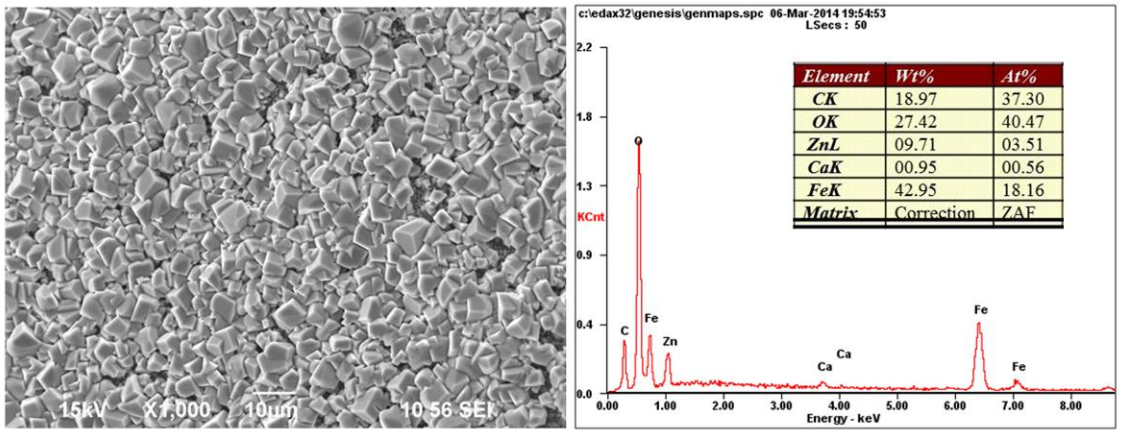

(a) (b)

Figure 17: SEM image (a) and EDS spectra (b) of the sandblasted rebar surface exposed to a pH 6.6 solution at 80ºC for 66 hours.

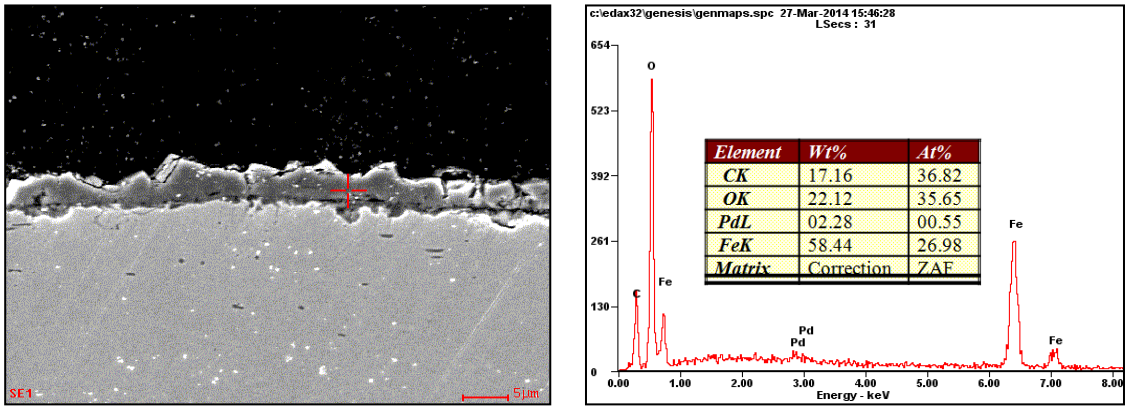

(a) (b)

Figure 18: SEM image (a) and EDS spectra (b) of the sandblasted rebar cross-section exposed to a pH 6.6 solution at 80ºC for 66 hours.

Figure 19 shows the variations of corrosion rate and OCP with time for the sandblasted rebar specimen with $FeCO_3$ exposed to the service conditions. The corrosion rate of this specimen slightly increased with time from 0.05 mm/y to 0.08 mm/y and the OCP value decreased with time. Comparing with other conditions shown in Figure 5 and Figure 12, it showed a significantly lower corrosion rate in the service conditions. This indicates that the $FeCO_3$ layer can give better protection in the absence of mill scale.

The steel rebar specimen surface exposed to the service conditions shows development of clusters of small globular-shaped pseudo-cubic crystals deposited on top of the prismatic iron carbonate crystals. These clusters of crystals tend to accumulate and form mounds and craters as demonstrated in Figure 20. The EDS analysis of the smaller pseudo-cubic crystals showed a higher intensity oxygen (O) peak and lower intensity carbon (C) peak, compared to the EDS analysis of the larger prismatic crystals, which gives a good indication of the presence of iron oxide. The presence of $FeCO_3$ provided some protection to the steel surface, hence the drop in the corrosion rate as demonstrated in the electrochemical measurements. In the meantime, the $FeCO_3$ layer was perturbed by iron oxide formation due to the presence of oxygen in the service conditions.[14,16]

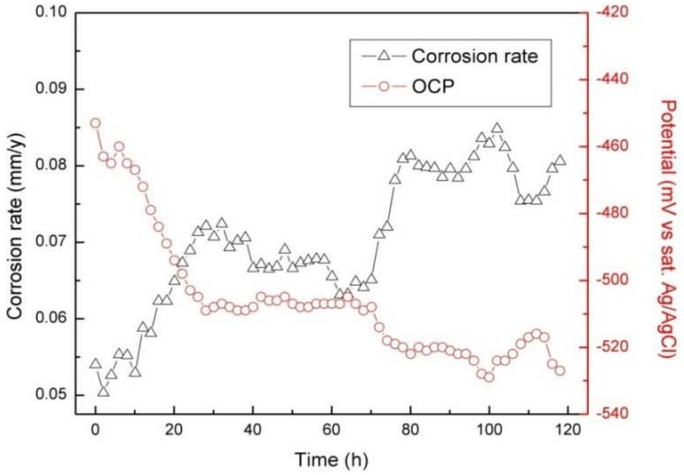

Figure 19: Variations of corrosion rate and corrosion potential with time for the steel rebar under service conditions (3.5 wt.% NaCl, pH 8.5, 25°C).

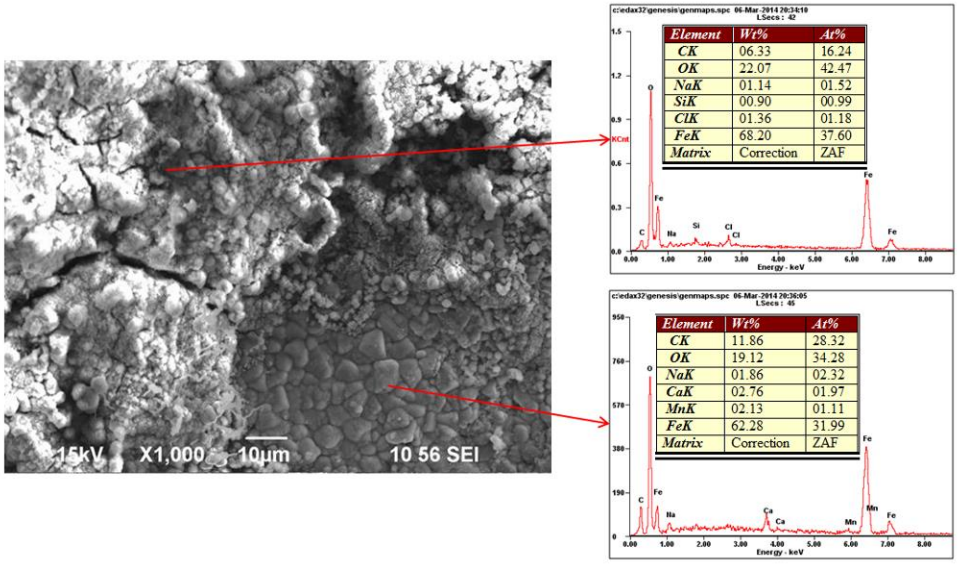

Figure 20: SEM image and EDS spectra of the surface of the sandblasted rebar with $FeCO_3$ exposed to the service conditions for 120 hours.

The cross-sectional view of the corrosion product on the steel surface shows a dome-like hollow tubercular structures (Figure 21).

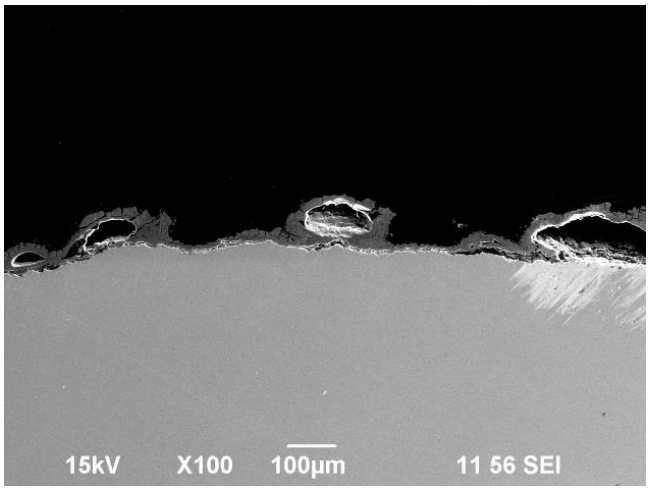

Figure 21: SEM image of the cross-section of the sandblasted rebar with $FeCO_3$ exposed to the service conditions for 120 hours.

The corrosion behavior of a sandblasted steel rebar (without $FeCO_3$) was also evaluated in the service condition. The corrosion rate and OCP changes with time are plotted in Figure 22. It is interesting to note that the corrosion rate decreased with time and stabilized on a low value (~ 0.12 mm/y) without the presence of $FeCO_3$. The corrosion potential increased with time and then stabilized.

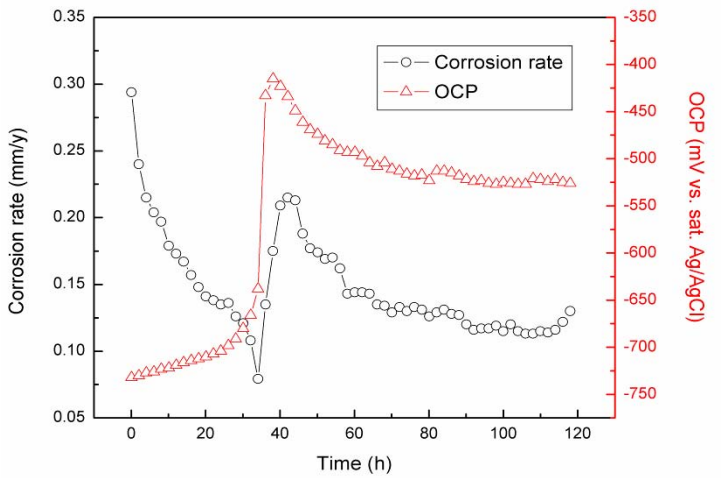

Figure 22. Variations of corrosion rate and corrosion potential with time for the sandblasted steel rebar under service conditions (3.5 wt.% NaCl, pH 8.5, 25°C).

Figure 23 shows the variation of corrosion rates with time in the service conditions for each of the different surface states. It clearly shows that the sandblasted rebar with the $FeCO_3$ coating has the lowest corrosion rate in the service conditions. It is also observed that the corrosion rates of specimens with mill scale (condition 1, 2 and 3) show a similar value, indicating some level of protection due to the presence of mill scale.

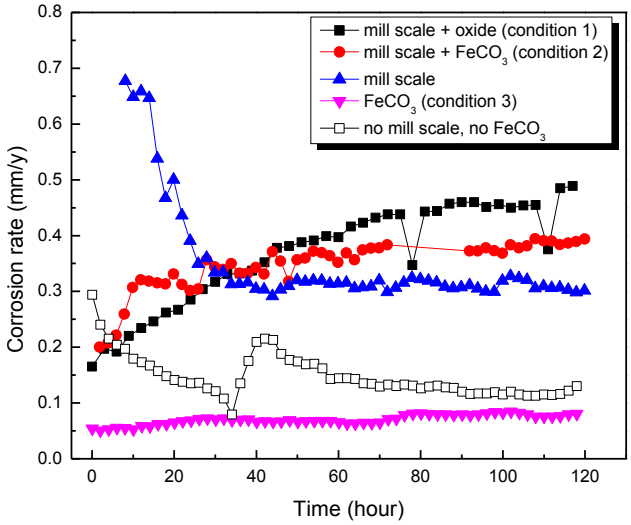

Figure 23: Variations of corrosion rates with time for the steel rebars under service conditions (3.5 wt.% NaCl, pH 8.5, 25ºC).

CONCLUSIONS

The conditions to form a protective $FeCO_3$ layer on reinforcement steel were simulated by controlling solution chemistry, temperature, and surface conditions. The corrosion characteristics of rebar with $FeCO_3$ layers formed under different conditions were evaluated in the simulated service conditions. The following conclusions are drawn:

- $FeCO_3$ formed on different rebar surfaces provides a certain degree of protection to the steel.
- $FeCO_3$ formed on sandblasted rebar indicated the lowest corrosion rates (0.05 to 0.10 mm/y) under the service conditions.
- The other surface conditions with a mill scale present had similar corrosion rates in excess of 0.3 mm/y, indicating some degree of protection by the mill scale.

ACKNOWLEDGMENTS

The authors would like to acknowledge the financial support from Solidia Technologies for the Institute for Corrosion and Multiphase Technology at Ohio University. The Center of Electrochemical Engineering Research at Ohio University is also thanked for assistance with acquisition of the Raman spectroscopy data.

REFERENCES

1. M.S. Imbabi, C. Carrigan, S. McKenna, “Trends and Developments in Green Cement and Concrete Technology,” *International Journal of Sustainable Built Environment* 1 (2012): p. 194.
2. A.C. Ramirez, “Evaluating Corrosion Resistance of Reinforcing Steel in a Novel Green Concrete,” MS thesis, (University of South Florida, 2015).
3. V. Atakan, S. Sahu, S. Quinn, X. Hu, N. DeCristofaro, “Why CO_2 Matters— Advances in a New Class of Cement,” *ZKG Int.* 67 (2014): p. 60.
4. E. Gartner, H. Hirao, “A Review of Alternative Approaches to the Reduction of CO_2 Emissions Associated with the Manufacture of the Binder Phase in Concrete,” *Cement and Concrete Research* 78 (2015): p. 126.
5. Z.T. Park, Y.S. Choi, J.G. Kim, L. Chung, “Development of a Galvanic Sensor System for Detecting the Corrosion Damage of the Steel Embedded in Concrete Structure: Part 2. Laboratory

Electrochemical Testing of Sensors in Concrete," *Cement and Concrete Research* 35 (2005): p. 1814.
6. Y.S. Choi, J.G. Kim, K.M. Lee, "Corrosion Behavior of Steel Bar Embedded in Fly Ash Concrete," *Corrosion Science* 48 (2006): p. 1733.
7. S. Nesic, K.-L. Lee, "A Mechanistic Model for Carbon Dioxide Corrosion of Mild Steel in the Presence of Protective Iron Carbonate Films-Part 3: Film Growth Model," *Corrosion* 59 (2003): p. 616.
8. S. Nesic, "Key Issues Related to Modelling of Internal Corrosion of Oil and Gas Pipelines – A Review," *Corrosion Science* 49 (2007): p. 4308.
9. W. Sun, S. Nesic, R.C. Woollam, "The Effect of Temperature and Ionic Strength on Iron Carbonate ($FeCO_3$) Solubility Limit," *Corrosion Science* 51 (2009): p. 1273.
10. E. Akeer, B. Brown, S. Nesic, "The Influence of Mild Steel Metallurgy on the Initiation of Localized CO_2 Corrosion in Flowing Conditions," CORROSION 2013, paper no. 2383 (Houston, TX: NACE, 2013).
11. W. Li, Y. Xiong, B. Brown, K. E. Kee, S. Nesic, "Measurement of Wall Shear Stress in Multiphase Flow and its Effect on Protective $FeCO_3$ Corrosion Product Layer Removal," CORROSION 2015, paper no. 5922 (Houston, TX: NACE, 2015).
12. F. Farelas, B. Brown, S. Nesic, "Iron Carbide and its Influence on the Formation of Protective Iron Carbonate in CO_2 Corrosion of Mild Steel," CORROSION 2013, paper no. 2291 (Houston, TX: NACE, 2013).
13. V. Fajardo, B. Brown, D. Young, S. Nesic, "Study of the Solubility of Iron Carbonate in the Presence of Acetic Acid using an EQCM," CORROSION 2013, paper no. 2452 (Houston, TX: NACE, 2013).
14. N.R. Rosli, Y.S. Choi, D. Young, "Impact of Oxygen Ingress in CO_2 Corrosion of Mild Steel," CORROSION 2014, paper no. 4299 (Houston, TX: NACE, 2014).
15. P. Ghods, O.B. Isgor, G.A. McRae, J. Li, G.P. Gu, "Microscopic Investigation of Mill Scale and its Proposed Effect on the Variability of Chloride-Induced Depassivation of Carbon Steel Rebar," *Corrosion Science* 53 (2011): p. 946.
16. N.R. Rosli, Y.S. Choi, S. Nesic, D. Young, "Corrosion of UNS G10180 Steel in Supercritical and Subcritical CO_2 with O_2 as a Contaminant," CORROSION 2016, paper no. 7527 (Houston, TX: NACE, 2016).